Absolute total, one-, two-, and three-electron-transfer cross sections for Ar^{q+} ($8 \leq q \leq 16$) on Ar at $2.3q$ keV

J. Vancura, J. J. Perotti, J. Flidr, and V. O. Kostroun
Nuclear Science and Engineering Program, Ward Laboratory, Cornell University, Ithaca, New York 14853
(Received 9 August 1993)

Absolute values for the total, one-, two-, and three-electron-transfer cross sections for Ar^{q+} ions ($8 \leq q \leq 16$) colliding with argon at $2.3q$ keV laboratory energy were measured by the growth-rate method. The Ar^{q+} ions were produced by the Cornell superconducting solenoid, cryogenic electron-beam ion source (CEBIS) and extracted at 2.3 kV. Selected charge states traversed a gas cell, after which they were detected and charge-state analyzed by the energy-retardation method and by a $\pi/\sqrt{2}$ cylindrical electrostatic analyzer. The target gas pressure in the cell was measured directly by the orifice flow method used for absolute pressure-gauge calibration. The overall error in the Ar^{q+} on Ar cross-section measurements is $\pm 10\%$.

PACS number(s): 34.70.+e, 82.30.Fi, 82.20.Pm

I. INTRODUCTION

The dominant process in low-energy, highly charged ion-atom collisions is electron capture. Over the past two decades, the number and degree of sophistication of experiments designed to investigate this fundamental process has been growing. The sheer quantity of papers devoted to this process attests to its importance and interest. Yet, in spite of the large amount of data on highly charged, ion-atom (molecule) collisions presently available, the number of measurements of absolute total and partial cross sections is relatively small. This is especially true for ion projectiles of charge q greater than ten and incident on almost any target.

Absolute total and partial cross sections provide one of the simplest and most direct comparisons between theory and experiment. They can be used to place relative data on an absolute scale, to connect different pieces of information such as the target recoil-ion charge-state distribution to the cross section for electron emission in a collision, or to check the internal consistency of different sets of data. Accurate and precise values of total and partial cross sections can signal the onset of different processes, or reveal subtle dependencies of the cross section on collision conditions.

A few measurements of absolute total, one-, and two-electron-transfer cross sections for low-velocity, ($v \ll 1$ a.u.), very highly charged argon ions incident on multielectron atoms have been reported in the literature. Klinger, Muller, and Salzborn [1] measured one to several electron transfer cross sections for Ar^{q+} ($2 \leq q \leq 7$) on Ar in the $5-15q$-keV collision energy range. Aubert *et al.* [2] measured one-electron-transfer cross sections for Ar^{q+} ($2 \leq q \leq 12$) on Ar in the $1-10q$-keV range. Justiniano *et al.* [3] measured charge transfer and ionization in Ar^{q+} ($2 \leq q \leq 9$) on Ne collisions in the $0.1-1.1q$-keV range.

In this paper, we report on a measurement of the absolute total, one-, two-, and three-electron-transfer cross sections for Ar^{q+} ($8 \leq q \leq 16$) on Ar at $2.3q$ keV. The cross sections include all processes which result in an argon projectile final charge state that is one, two, or three units lower than the incident charge state.

In a previous paper [4] we reported on similar measurements of absolute total, one- and two-electron transfer cross sections for Ar^{q+} on H_2 and He. The present measurements were motivated by our investigations of multielectron transfer between low-energy, highly charged ions and medium-Z atomic and molecular targets. Since Ar^{q+} on Ar and Ar^{q+} on H_2 and He are fundamentally quite different collision systems, the question arose as to what extent, if at all, total, one- and two-electron-transfer cross sections reflect differences among these systems. The variation of the transfer cross sections with a charge state for a given collision system provides one such means for comparison, and the precision of the data is at the level where apparent deviations in the shape of the cross section from one system to another might be significant.

II. EXPERIMENTAL METHOD

The absolute total and one- and two-electron-transfer cross sections were measured by the growth-rate method [5]. In this method, a beam of ions of charge q traverses a gas cell of length l and a target density of n atoms/cm^3. Due to charge-changing collisions, new charge-state fractions are produced. The growth of the different ion charge states with increasing pressure and the decrease of the incident projectile charge state are recorded. The cross sections are then determined from the measured charge-state vs pressure dependence.

The large disparity in the magnitudes of the one-, two-, and three-electron-transfer cross sections requires that some care be exercised in the measurement. In particular, the predominance of the one electron transfer over two- and three-electron-transfer cross section introduces large uncertainties in the latter values. It is customary to measure atomic cross sections under conditions that satisfy the single-collision criterion [5]. This criterion

can always be satisfied by making the target tenuous enough, although at some point the product signal becomes too weak and the background gas pressure introduces a nonnegligible contribution. In the measurements described below, it is possible to have a linear variation with pressure for the one-electron-transfer cross section, and at the same time a nonlinear variation for the two- and three-electron-transfer cross sections. Furthermore, the nonlinear contribution can be comparable to the linear contribution even at very low pressures as can be calculated from expressions (1) and (2) below. The problem of multiple collision which masquerade as double- and triple-electron capture cannot be circumvented by the use of other, e.g., coincidence, techniques.

In Ref. [4] we obtained exact expressions for the evolution of the product charge-state distributions with gas target thickness when the projectile charge state q either remains the same or changes to $q-1$ or $q-2$. Since we were dealing with two-electron targets only, any observation of projectiles that had captured more than two electrons unambiguously signaled multiple-collision conditions and there was no reason to evaluate the rather complicated expressions further. However, in the present experiment this is not the case and it is necessary to evaluate the multiple-collision contribution in greater detail. In order to obtain suitable expressions, we look at the same problem from a slightly different point of view.

Let $\sigma_{q,t}$ be the total cross section for one-, two-, etc., electron-transfer to an ion of charge q. During the collision, the projectile may capture anywhere from one to several electrons. However, only one, two, or three electrons are permanently transferred from the target to projectile, and these charge-changed projectiles are the ones actually detected in an experiment. Similarly, let $\sigma_{q,q-1}\equiv\sigma_{q,1}$ be the one-electron-transfer cross section, $\sigma_{q,q-2}\equiv\sigma_{q,2}$ the two electron-transfer cross section and so on. The probability that an ion of charge q undergoes a collision which decreases its charge by one unit in a distance dx after it has traversed a distance x is $\Sigma_{q,1}dx$, where $\Sigma_{q,1}\equiv\sigma_{q,1}n$ and n is the number of target atoms (molecules) per unit volume. It follows that the probability that an ion of charge q survives traversing a distance x without undergoing any collision is $e^{-\Sigma_{q,t}x}$. The probability $P^1_{q,q-1}(l)$ that an ion of charge q undergoes one and only one collision that decreases its charge by one unit when it traverses a distance l is then

$$P^1_{q,q-1}(l)=\int_0^l \exp(-\Sigma_{q,t}x)\times\Sigma_{q,1}dx\exp[-\Sigma_{q-1,t}(l-x)]\ . \quad (1)$$

Similarly, the probability $P^2_{q,q-2}(l)$ that an ion of charge q will undergo two and only two collisions each of which decreases its charge by one unit is

$$P^2_{q,q-2}(l)=\int_0^l P^1_{q,q-1}(x)\Sigma_{q-1,1}dx\exp[-\Sigma_{q-2,t}(l-x)] \quad (2)$$

and so on. Carrying out the integrations in (1), and taking the arguments in the exponentials that are small compared to one, the single-collision condition, gives

$$P^1_{q,q-1}(l)=\Sigma_{q,1}l-\tfrac{1}{2}\Sigma_{q,1}(\Sigma_{q,t}+\Sigma_{q-1,t})l^2 \quad (3)$$

and

$$P^1_{q,q-2}(l)+P^2_{q,q-2}(l)=\Sigma_{q,2}l+\tfrac{1}{2}[\Sigma_{q,1}\Sigma_{q-1,1}-\Sigma_{q,2}(\Sigma_{q,t}+\Sigma_{q-2,t})]l^2\ . \quad (4)$$

These equations are the same as Eq. (3) of Ref. [4]. In the present case, we are also interested, in addition to the above, in $P^1_{q,q-3}(l)$, $P^2_{q,q-3}(l)$, and $P^3_{q,q-3}(l)$, where

$$P^2_{q,q-3}(l)=\int_0^l[P^1_{q,q-2}(x)+P^2_{q,q-2}(x)]\times\Sigma_{q-2,1}dx\exp[-\Sigma_{q-3,t}(l-x)] \quad (5)$$

and similarly for $P^3_{q,q-3}(l)$. Only $P^1_{q,q-3}(l)$ contains the linear term $\Sigma_{q,3}l$. These and similar expression can easily be evaluated by computer algebra systems software packages such as Maple [6] or *Mathematica* [7] to assess the multiple-scattering contributions under given experimental conditions. The cross sections were extracted from the projectile charge-state variations with target thickness by least squares fitting the $\sigma_{q,1}$ data to a linear function, and the $\sigma_{q,2}$,$\sigma_{q,3}$ data to a quadratic function.

A. Experimental arrangement

Low-energy, metastable free, highly charged argon ions were produced by the Cornell superconducting solenoid, cryogenic electron-beam ion source [8]. The ions were extracted at 2.3 kV, and charge-state analyzed by a 90° bending magnet. The experimental arrangement used to measure the cross sections is identical to that described in [4]. The charge-selected ions entered a gas cell, and after exiting from the gas cell, the ion beam was again charge-state analyzed either by a system of retarding grids [5,9] or by a $\pi/\sqrt{2}$ cylindrical electrostatic analyzer. The ions were detected by a shielded Faraday cup located behind the retarding grids, or by a high-current channeltron electron multiplier placed behind the $\pi/\sqrt{2}$ cylindrical electrostatic analyzer exit slit.

The effective gas cell target thickness was determined from the absolute pressure in the gas cell and its dimensions. The former was measured directly in the cell by the orifice flow method used for absolute pressure-gauge calibration [10,11]. Briefly, the gas cell consists of two cylindrical chambers, of which the lower is the target cell. The conductances of the ion-beam entrance and exit apertures give a total conductance C_2. Target gas at a pressure P_1 is admitted into the upper chamber which is separated from the lower chamber by a very small conductance C_1. For vacuum system background pressures that are small compared to the pressure P_c in the gas cell, P_c is given by

$$P_c=\frac{P_1}{(1+C_2/C_1)}\ , \quad (6)$$

where C_2/C_1 is known [4], and the absolute pressure P_1 is measured with a MKS Baratron model 222B capacitance manometer [12]. The error in the absolute pressure

P_c in the cell is estimated to be 2.5% [4].

The major uncertainty in determining the gas target thickness is the effective length of the gas cell. We took the effective length to be the actual length of the gas cell, 12.2 cm, plus the sum of the entrance and exit aperture diameters. The entrance and exit aperture diameters are 0.4 and 0.5 cm, respectively, and the apertures are 0.05 cm thick. This introduces a maximum uncertainty of 7.4% in the gas target thickness. The variation of the vacuum chamber background pressure with gas target cell pressure is shown in Fig. 1. Since the distance from the gas cell exit slit to the detector is 2.2 times the length of the cell, the background pressure contribution is negligible over the target cell pressure range used in the experiment.

B. Ion-beam measurements

Cross-section measurements require that the beam intensity of the various charge-state fractions present be known accurately. The ions leaving the gas cell were detected either by a Faraday cup or by a channeltron electron multiplier operated in the current mode. The Faraday cup intercepted ions scattered by $\pm 2.5°$, so that all projectiles scattered in capture were collected. The design of the Faraday cup and its large length to diameter ratio ensure that the secondary electrons are collected if the ion beam is centered.

The channeltron output current was amplified by a Keithley 127 current to voltage amplifier. The output from the Keithley was then fed into a Tektronix 2430A digital oscilloscope for processing. The ion current recorded by the channeltron electron multiplier was also corrected for the response of the multiplier to different charge states which produce different amounts of secondary electrons. This correction is discussed in Ref. [4].

III. RESULTS

A. Cross-section measurements and data analysis

For each projectile charge state q, the variation with pressure of the $(q-1)$, $(q-2)$, and $(q-3)$ product ion was recorded, Fig. 2. In addition, six retarding energy scans were taken at a gas cell pressure of 4.32×10^{-5} mbar. From the retarding grid voltage scans the fraction of ions whose charge had changed to $(q-1)$, $(q-2)$, or $(q-3)$, that is N_{q-1}/N_q, N_{q-2}/N_q, and N_{q-3}/N_q were determined, where N_{q-1} is the number of ions of charge $q-1$, etc., and N_q is the number of primary beam ions.

To record the pressure dependence, the $\pi/\sqrt{2}$ cylindrical electrostatic analyzer was set to select a $(q-1)$, $(q-2)$, or $(q-3)$ product ion. Then the pressure in the upper reservoir, measured by a Baratron capacitance manometer, was allowed to increase at a rate of 1 to 2 mbar/s. [The pressure increase in the gas cell is related to the pressure increase in the upper reservoir by Eq. (6).] At this rate, the rise was slow enough to allow the pressure in the gas cell to come to equilibrium. The ion signal from the $\pi/\sqrt{2}$ cylindrical electrostatic analyzer channeltron and the Baratron pressure signal were recorded together. The channeltron bias high voltage

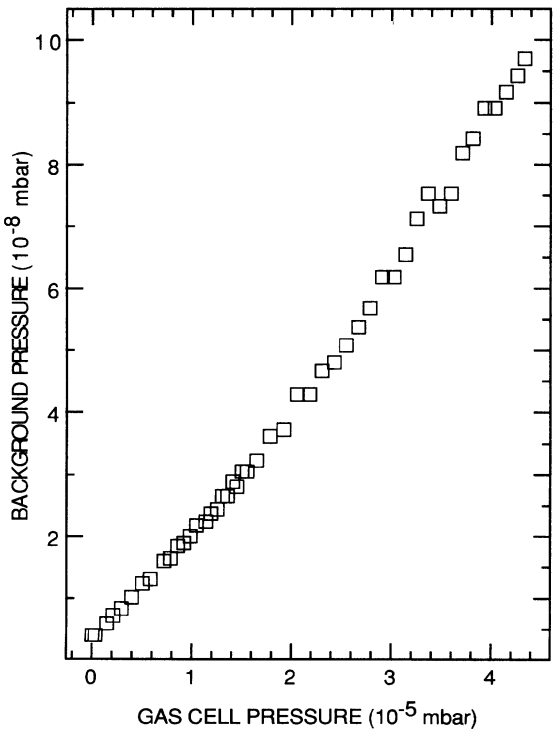

FIG. 1. Variation of vacuum-system background pressure with gas target cell pressure. Within the pressure range used in the experiment, the ratio of the cell to background pressure was around 500 to 1.

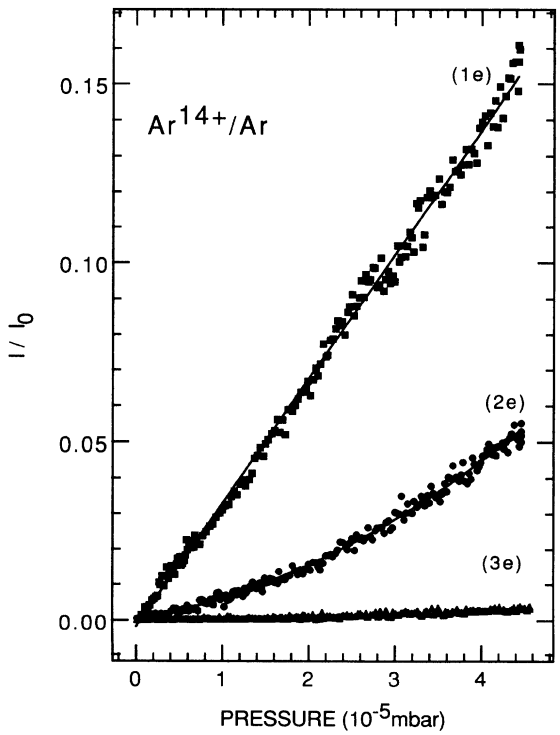

FIG. 2. One-, two-, and three-electron-transfer charge fraction growth with pressure for Ar^{14+} on Ar as measured with the $\pi/\sqrt{2}$ cylindrical electrostatic analyzer. The data are corrected for the response of the channeltron to different charge states.

was maintained at 1000–1800 V (depending on the ion-beam intensity) to keep the current flowing through the channeltron below 1 μA and thereby prevent its saturation. In addition, the ion beam through the gas cell was monitored via the beam intercepted by the grids used in the energy-retarding measurements. These data provided a check on the stability of the ion beam.

The pressure variation with time data, typically 150–250 data points, were then least squares fitted to either a linear or quadratic function. Once the coefficients of the least-squares fit had been determined, the relative value of the ion signal was established at 4.32×10^{-5} mbar, the maximum pressure in the target cell. By equating this value to the absolute ion signal obtained from the retarding energy scan at the same pressure, the overall pressure variation was tied down to an absolute scale. The data sets were then again least squares fitted to the same function, and the cross sections are the resulting coefficients of the fits. In Fig. 2, the $\sigma_{q,1}$ data were fitted to a linear function, while the $\sigma_{q,2}$ and $\sigma_{q,3}$ data were fitted to a quadratic function. Since $\sigma_{q,1}$, $\sigma_{q-1,1}$, $\sigma_{q,t}$ etc., are all on the order of 1.0×10^{-14} cm^2, and $\sigma_{q,2}$ is a factor of 10 smaller, at a target thickness of 1.3×10^{13} atoms/cm^2 (corresponding to a pressure of 4.32×10^{-5} mbar and a 12.2-cm cell length), the linear term in (3) is typically a factor of 10 greater than the quadratic term. In Eq. (4), the linear term, proportional to $\sigma_{q,2}$ is only a factor of 2–3 greater than the quadratic term. From (5) we get that the linear term, proportional to $\sigma_{q,3}$, is only one fifth of $P^2_{q,q-3}(l)+P^3_{q,q-3}(l)$ at the same pressure.

The results are summarized in Table I and plotted in Fig. 3. The errors consist of the errors in the coefficients of the least-squares fit, and the errors in the signal, cell pressure, and effective cell length. In addition to our values, we also list in Table I the cross sections, together with their errors, measured by Aubert *et al.* [2]. Since the values were not stated explicitly, we extracted them from the graphs in the article.

The retarding energy grid voltage scans gave very precise N_{q-1}/N_q and $(N_{q-2}+N_{q-3})/N_q$ values. However, difficulties arose with the determination of N_{q-3}/N_q. Even at the relatively high pressure of 4.32×10^{-5} mbar, this ratio is on the order of 10^{-3}, and the N_{q-3} signal is comparable to noise. In this case we used $\pi/\sqrt{2}$ cylindrical electrostatic analyzer scans at 4.32×10^{-5} mbar to breakup $(N_{q-2}+N_{q-3})/N_q$ into its individual components. As in Ref. [4], we have assumed that the relative response of the channeltron of charge state $(q-1)$ relative to q, $R_{q/q-1}$, was such that $R_{q/q-1}/R_{q/q-2}=R_{q/q-2}/R_{q/q-3}$. For $8\le q\le16$, the $R_{q/q-1}$ etc., ratios varied only slightly between 1.2 and 1.4. This assumption is quite good for estimating $\sigma_{q,q-3}$. It should be noted that a 20% error in the sensitivity ratio would result in approximately a 20% error in $\sigma_{q,q-3}$, but only a 2% error in $\sigma_{q,q-2}$ since their ratio $\sigma_{q,q-3}/\sigma_{q,q-2}$ is usually around $\frac{1}{10}$.

B. Comparison with other experiments

Figure 4 compares our $\sigma_{q,q,1}$ cross sections for Ar^{q+} on Ar, solid circles, with the $\sigma_{q,q-1}$ measurements of Au-

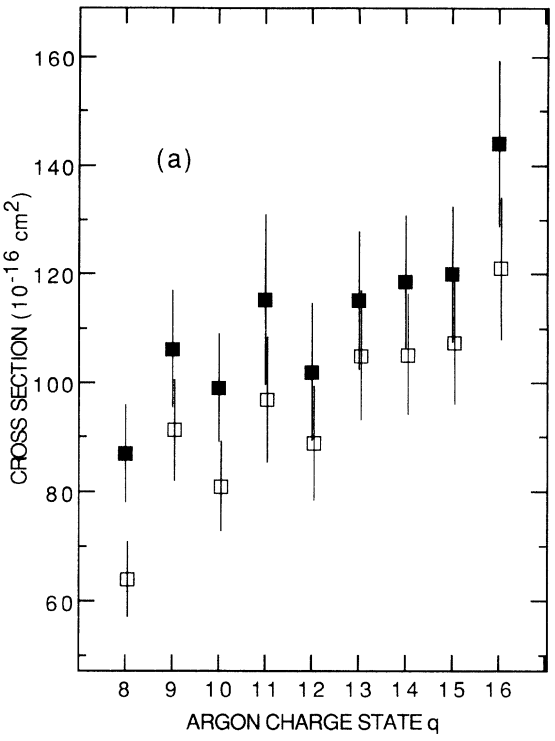

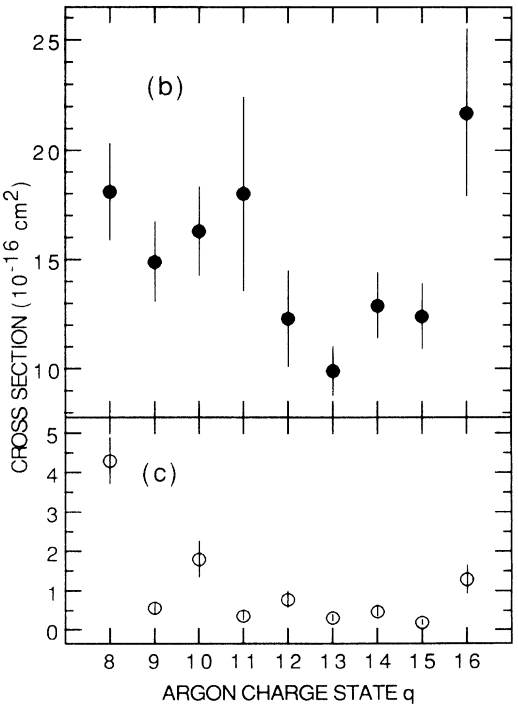

FIG. 3. (a) Measured total- (solid squares) and one-electron- (open squares) transfer cross sections for Ar^{q+} on Ar at $2.3q$ keV as a function of argon projectile charge state q, and (b) two-electron- (solid circles), and (c), three-electron- (open circles) transfer cross sections.

TABLE I. Ar^{q+} on Ar cross sections at $2.3q$ keV (10^{-16} cm^2).

	$\sigma_{q,q-1}$				
q	This work	Ref. [2][a]	$\sigma_{q,q-2}$	$\sigma_{q,q-3}$	$\sigma_{q,\mathrm{tot}}$
8	64.0±6.8	40.1±8.0	18.1±2.2	4.3±0.58	86.4±8.8
9	91.3±9.2	58.0±11.6	14.9±1.8	0.57±0.14	106.7±10.7
10	81.0±8.1	53.5±10.7	16.3±2.0	1.80±0.45	99.1±10.0
11	96.9±11.5	56.1±11.2	18.0±4.4	0.36±0.10	115.3±15.6
12	88.9±10.4	66.7±13.3	12.3±2.2	0.79±0.20	102.0±12.6
13	105.0±11.9		9.9±1.1	0.31±0.08	115.2±12.6
14	105.2±11.1		12.9±1.5	0.48±0.12	118.6±12.1
15	107.4±11.3		12.4±1.5	0.19±0.05	120.0±12.4
16	121.1±13.0		21.7±3.8	1.30±0.34	144.1±15.2

[a]Evaluated at $2.3q$ keV.

bert *et al.*, solid triangles [2]. The same figure also shows the data of Klinger, Muller, and Salzborn [1] for lower q values, open triangles. Although the data of Klinger, Muller, and Salzborn [1] do not cover the higher charge states, one can see from Fig. 4 that the data follow the same trend as ours. The Aubert *et al.* [2] data are consistently lower than our data and that of Klinger, Muller, and Salzborn [1]. The most likely reason for the discrepancy between our data and that of Ref. [2] is the manner in which the pressure in the collision chamber was measured and the rather high background pressure taken into account in Ref. [2]. Both Klinger, Muller, and Salzborn [1] and Aubert *et al.* [2] measured the target gas pressure with an ionization gauge. However, the ionization gauge is not an absolute gauge and its sensitivity depends on the composition of gases present. It must, therefore, be calibrated for a known gas and its relative sensitivity for other gases must be determined [13,14]. Klinger, Muller, and Salzborn [1] do state that their gauge was calibrated against a commercial high-precision calibration tube, while Aubert *et al.* [2] do not mention any gauge calibration. A factor of 1.3 [14], the relative sensitivity to Ar of an ion gauge calibrated for N_2, would bring the Aubert *et al.* data more in line with our data.

In the Aubert *et al.* [2] experiment, the pressure outside the cell was always only one order of magnitude or so lower than in the collision chamber. (Compare this with our Fig. 1.) Therefore, the background contribution had to be subtracted from the total ion signal. However, because of the dependence of the ionization gauge sensitivity on vacuum system gas composition, the correction method applied by Aubert *et al.* [2] to the measured total ion signal while fine in principle, may not be reliable in practice.

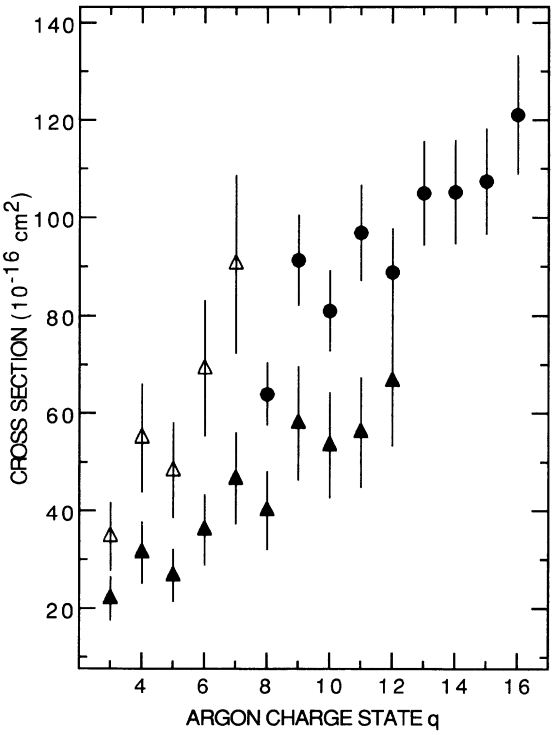

FIG. 4. Comparison of our one-electron-transfer cross-section data for Ar^{q+} on Ar at $2.3q$ keV (solid circles), with one-electron-transfer cross sections measured by Klinger, Muller, and Salzborn [1] (open triangles) and those of Aubert *et al.* [2] (solid triangles).

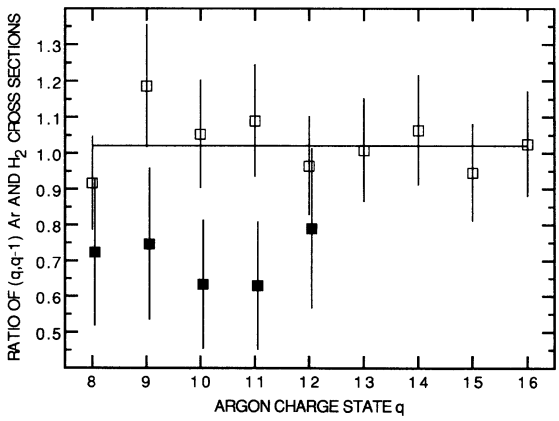

FIG. 5. Ratio of measured Ar^{q+} on Ar to Ar^{q+} on H_2 one-electron-transfer cross sections versus argon projectile charge state q. Open squares represent present Ar^{q+} on Ar data and Ar^{q+} on H_2 data taken from our previous work [4]. Solid squares represent the ratio of Ar^{q+} on Ar data of Aubert *et al.* [2], to the Ar^{q+} on D_2 data measured by the same group, Bliman *et al.* [15]. The straight line is the ratio of Ar (15.755 eV) to H_2 (15.427 eV) ionization potentials [16].

As a check on the consistency of both our data, and that of Aubert *et al.* [2], we have plotted the ratio of the $\sigma_{q,q-1}$ cross sections for Ar^{q+} on Ar to that of Ar^{q+} on H_2 as a function of q, Fig. 5. Our ratio of the Ar $\sigma_{q,q-1}$ cross sections obtained in this experiment to the H_2 cross sections given in Ref. [4] is close to one, whereas the ratio of the argon cross sections obtained by Aubert *et al.* [2] to their D_2 cross sections Ref. [15] is around 0.7. Since their Ar^{q+} on D_2 cross sections are more in line with out values, this is another indication that their Ar^{q+} on Ar one-electron-transfer cross sections are too low.

IV. DISCUSSION

The magnitudes of total cross sections for Ar^{q+} on Ar, and Ar^{q+} on H_2 and He collision systems suggest that encounters in which nuclei pass one another at distances of 3.6–6.7 Å result in the transfer of one or more electrons to the projectile. However, as pointed out some time ago [17], the final projectile is not an indication of the actual number of electrons transferred from the target to the projectile during the collision. A more accurate indication of this number, at least for the low-energy highly charged ion-atom (molecule) collisions under consideration, is the charge on the recoil ion [18].

The variations of cross sections with projectile charge q, combined with the corresponding recoil ion charge-state variations can provide some insight into the process of electron capture. Figure 6(a) shows the scattered projectile charge fractions obtained from measured cross sections [4] for Ar^{q+} on H_2 collision as a function of q. Collisions in which projectiles have retained one-electron account for more than 97% of all collisions. In 2–3 % of the collisions the argon projectiles captured and retained two electrons. One-electron transfer to the projectile can result from normal one-electron capture and from two-electron capture followed by autoionization. Two-electron-transfer results from two-electron capture followed by radiative deexcitation.

As far as we know, the ratio of probabilities for two-electron to one-electron capture from H_2 has not been determined thus far. One might think that this quantity is given by the ratio of protons to H_2^+ ions observed in Ar^{q+} on H_2 collisions. Unfortunately, protons can arise from both double and single capture from H_2. Single capture may excite the residual H_2^+ ion which then dissociates into H^+ and H [19]. Transfer ionization, or the capture of two electrons by a projectile into a state that deexcites by autoionization cannot be distinguished from normal one-electron capture in total cross-section experiments. However, the variation of the $q-1$ scattered projectile charge fraction with q, Fig. 6(a) indicates that whatever the relative distribution of single capture and transfer ionization is, it does not vary with the projectile charge state.

Figure 6(b) shows the scattered projectile charge fraction obtained from measured cross sections [4] for Ar^{q+} on He collisions as a function of q. The figure shows a drop in the $q-2$ fraction and a corresponding rise in the $q-1$ fraction as the argon projectile charge increases from 8+ to 9+. Coincidence measurements by Justiniano *et al.* [3] show a drop in normal double capture and an increase in transfer ionization from argon 8+ to 9+ on He. Using their data [3], we get for Ar^{8+} on He that $\sigma_{8,7}/\sigma_{8,\mathrm{tot}}=0.84\pm0.08$ and $\sigma_{8,6}/\sigma_{8,\mathrm{tot}}=0.16\pm0.02$, while for Ar^{9+}, $\sigma_{9,8}/\sigma_{9,\mathrm{tot}}=0.96\pm0.12$ and $\sigma_{9,7}/\sigma_{9,\mathrm{tot}}=0.03\pm0.01$. These values are consistent with our cross-section ratios shown in Fig. 6(b). Apart from Ar^{8+}, the average scattered projectile one- and two-electron-transfer fractions in Ar^{q+} on He collisions are 0.98±0.02 and 0.02±0.01, respectively. For Ar^{8+} the fractions are 0.73±0.07 and 0.27±0.03. If we take direct ionization of the target to be negligibly small at the projectile energies under consideration [17], the recoil-ion charge is an indication of the number of electrons captured by the projectile during the collision [18]. For the time being, we exclude, for lack of direct evidence, the possibility of target ionization due to Auger deexcitation of collisionally excited target states.

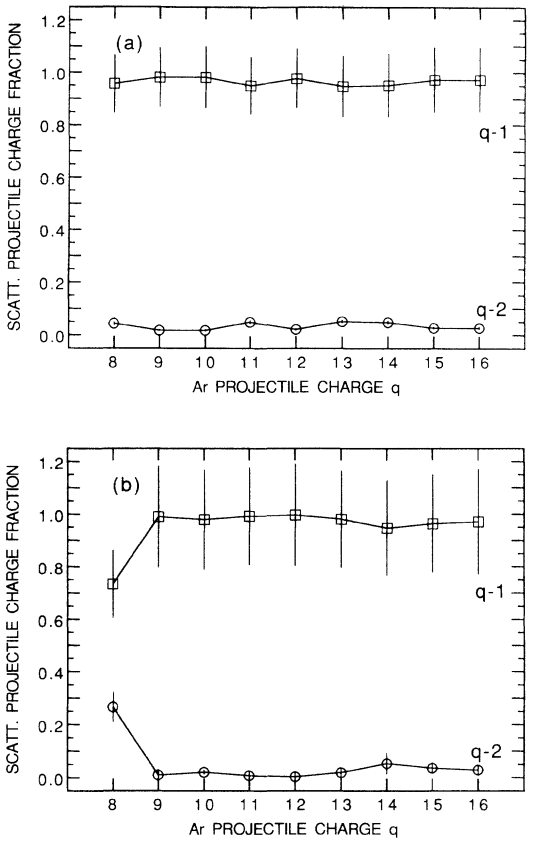

FIG. 6. (a) Scattered projectile charge fractions calculated from measured cross sections [4] for Ar^{q+} on H_2 collisions as a function of q. (b) Scattered projectile charge fraction obtained from measured cross sections [4] for Ar^{q+} on He collisions as a function of q.

The observed fractions of singly and doubly charged He recoils produced in $Ar^{8+,9+}$ on He collisions at $2.3q$ keV are 0.78±0.01 and 0.22±0.02, respectively, for Ar^{8+}, and 0.95±0.01 and 0.05±0.01 for Ar^{9+} [20]. From the Justiniano *et al.* data [3] we calculate that the fraction of singly and doubly charged He recoil fractions is 0.80±0.07 and 0.20±0.02, respectively, for Ar^{8+}, and

0.90 ± 0.11 and 0.10 ± 0.02 for Ar^{9+}.

Unfortunately, neither our recoil ion data, nor the Justiniano *et al.* coincidence data was extended beyond Ar^{9+} for the He target. However, from the general trend of scattered projectile charge fractions with q, Fig. 6(b), we can conclude that for $9 \leq q \leq 16$, normal double capture to an excited state of the projectile followed by radiative deexcitation is independent of the argon projectile charge q. A similar conclusion holds for the relative distribution of single capture to transfer ionization. With the exception of Ar^{8+}, the scattered projectile charge fraction q dependence in Ar^{q+} on H_2 and Ar^{q+} on He are almost identical.

Figure 7 shows the variation of scattered projectile $q-1$, $q-2$, and $q-3$ fractions with q as obtained from measured Ar^{q+} on Ar cross sections. For comparison, Fig. 8 shows the 1+, 2+, and 3+ recoil charge fractions as a function of q in Ar^{q+}on Ar collisions [21]. (These three charge states account for 80% of all recoil ions.) In Fig. 7, disregarding Ar^{8+} on Ar, the average fraction of scattered projectiles that have gained one electron is 0.865 ± 0.032, and those that have gained two and three electrons are 0.128 ± 0.028 and 0.006 ± 0.005, respectively.

By the same argument made above for He, the fraction of singly charged argon recoil ions, Fig. 8, is identical to the fraction of one-electron-capture collisions. If we subtract this fraction from the $q-1$ fractions in Fig. 7, we get the fractions labeled $(q-1)MC$, solid black squares, in the same figure. These represent the fraction of multiple captures that have resulted in a single electron being retained by the projectile. The average value of this fraction is about 0.4. If we combine it with the fractions labeled $q-2$ and $q-3$, which give the fractions of multiple captures that result in two and three electrons being retained by the projectile, we see that more than half, or about 57% of Ar^{q+} on Ar collisions involve multiple-electron capture. Thus normal single-electron capture occurs in less than half of the collisions.

Figures 7 and 8 show that both the recoil and scattered projectile charge fractions vary with projectile charge q. In particular, the recoil charge fractions for 1+ and 2+ show marked out of phase variations, i.e., as the fraction

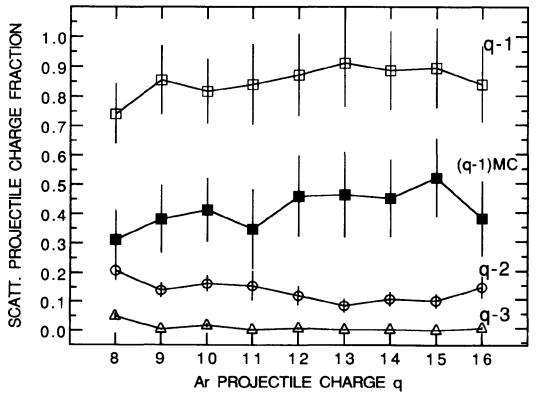

FIG. 7. The variation of scattered projectile $q-1$, $q-2$, and $q-3$ fractions with q as obtained from the Ar^{q+} on Ar cross sections measured in this experiment.

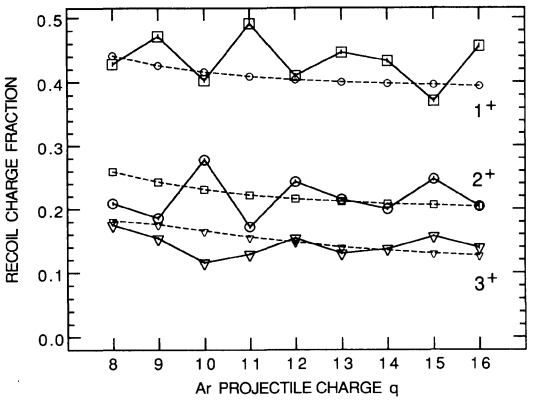

FIG. 8. The 1+, 2+, and 3+ recoil charge fractions as a function of q in Ar^{q+} on Ar collisions [21]. The dashed lines are the ratios of one-, two-, and three-electron capture to total capture cross sections according to the MCBM.

of singly charged recoils goes up, the fraction of doubly charged ones goes down and vice versa. The more highly charged recoils also show such variations. Ar^{8+} on Ar shows a smaller fraction of one-electron transfers than do the other Ar^{q+} projectiles. This is similar to what is observed in Ar^{8+} on He collisions.

As far as comparison of data with theory is concerned, at present there exists no quantum or semiclassical theory of inelastic collisions that treats multielectron capture from first principles. Instead, a number of models have been developed to provide some physical understanding of the experimental data. Approximate values of the capture radii can be estimated from a number of models such as the absorbing sphere [22,23], multichannel Landau-Zener [24], and classical over the barrier model [25,26]. All of these are based on the treatment of charge exchange between a hydrogen atom in its ground state and a bare heavy nucleus at collision velocities $v < 1$. The models are designed to handle projectiles other than bare nuclei and target ionization potentials different from hydrogen. Accordingly, they are really limited to descriptions of one-electron transfer, and treat all collision systems on an equal footing. By their very hydrogenic nature, they cannot be easily generalized to describe multielectron transfers.

However, if one assumes that the electrons involved in the collision behave independently, then it is possible to describe multielectron capture by the projectile within the general framework of the over barrier model. The molecular classical over barrier model (MCBM) [27] is a more sophisticated version of the over barrier model [25,26] which can account for the different ways whereby a given number of electrons can be exchanged between the target and the projectile. The model, which has no adjustable parameters, can be used to calculate absolute cross sections for the initial population of projectile charge states, and to predict the subsequent autoionization of either the projectile or the target. It can also predict the width of energy gain spectra, and angular distributions of the scattered projectile for different numbers of electrons captured by the projectile during the collision

[28]. Following Ref. [27], we have calculated MCBM cross sections $\sigma_{q-r}^{(j)}$ corresponding to the 2^8 eight-electron MCBM strings (j). These were grouped according to the number r of electrons, (0–8), captured by the projectile. The argon target ionization potentials I_i used in the MCBM calculations were computed using a multiconfiguration Hartree-Fock program [29]. The following values were obtained for $I_1 \ldots I_8$: 14.75, 27.40, 41.37, 56.54, 72.82, 90.16, 122.3, and 142.9 eV. The total cross section for a projectile of charge q incident on a target from which up to eight electrons can be removed is given by [27]

$$\sigma_q = \sum_{r=0}^{8} \sum_{(j)} \sigma_{q-r}^{(j)} , \tag{7}$$

where the inner sum extends over all possible strings (j) corresponding to r electrons captured by the projectile. This cross section is also equal to the geometrical cross section $\pi(R_1^{\text{in}})^2$, where R_1^{in} is the distance at which the least bound electron on the target becomes molecular on the incoming part of the trajectory.

Figure 9 shows a plot of the MCBM total capture cross section $\sigma_{q,t} = \sigma_q - \sigma_q^{(0)}$ as a function of q, together with our total cross-section data and that of Klinger, Muller, and Salzborn [1]. [$\sigma_q^{(0)}$ is the cross section for no charge transfer and corresponds to the string (0)=(000...0).] From the figure we see that the MCBM total cross section is significantly greater than our measured cross section, and that its overall variation with q is quite different.

The MCBM cross sections vary almost linearly with the projectile charge q, and appear to follow the Klinger, Muller, and Salzborn data [1]. However, as can be seen from the measured total cross sections in Fig. 9, and the one electron-transfer cross section in Fig. 4, (which also includes the Aubert *et al.* [2] data), the Klinger *et al.* data are not inconsistent with ours.

We do not compare the $\sigma_{q,q-1}$, $\sigma_{q,q-2}$, and $\sigma_{q,q-3}$ cross sections with the predictions of the MCBM calculations since this would require further assumptions regarding autoionizing transitions from excited projectile states formed in capture. Instead, we have calculated the ratios of one-, two-, and three-electron capture to total capture MCBM cross sections and compare these with measured recoil-ion charge fractions, Fig. 8, dashed lines. Assuming that the recoil-ion fractions are a reliable indication of the actual number of electrons transferred from the target to the projectile during the collision, the agreement in this case is quite impressive.

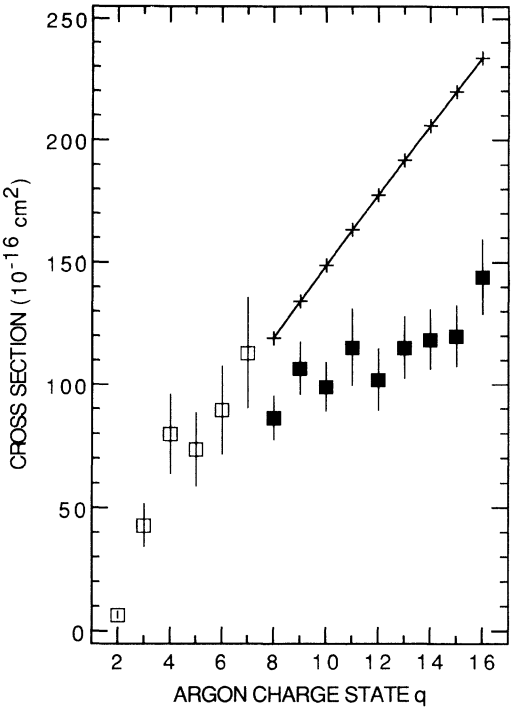

FIG. 9. Comparison of measured total Ar^{q+} on Ar cross sections with total cross sections calculated according to the molecular Coulomb over barrier model (solid line). Present data, solid squares; Klinger, Muller, and Salzborn [1], open squares.

ACKNOWLEDGMENT

This work was supported in part by the U.S. Department of Energy, Office of Basic Energy Sciences, Division of Chemical Sciences.

[1] H. Klinger, E. Muller, and E. Salzborn, J. Phys. B **8**, 230 (1975).
[2] J. Aubert, S. Bliman, R. Geller, B. Jacquot, and D. Van Houtte, Phys. Rev. A **22**, 2403 (1980).
[3] E. Justiniano, C. L. Cocke, T. J. Gray, R. D. DuBois, and C. Can, Phys. Rev. A **24**, 2953 (1981).
[4] J. Vancura, V. J. Marchetti, J. J. Perotti, and V. O. Kostroun, Phys. Rev. A **47**, 3758 (1993).
[5] H. Tawara and A. Russek, Rev. Mod. Phys. **45**, 178 (1973).
[6] Waterloo Maple Software, 160 Columbia St. West, Unit 2, Waterloo, Ontario, Canada N2L 3L3.
[7] Wolfram Research, Inc., 100 Trade Center Drive, Champaign, IL 61820.
[8] V. O. Kostroun, in the *Proceedings of the International Symposium on Electron Beam Ion Sources and their Applications,* edited by A. Hershcovitch, AIP Conf. Proc. No. 188 (AIP, New York, 1989), p. 65.
[9] V. F. Kozlov and A. M. Rozhkov, Zh. Tekh. Fiz. **32**, 719 (1962) [Sov. Phys. Tech. Phys. **7**, 524 (1962)].
[10] K. E. Poulter, J. Phys. E **10**, 112 (1977).
[11] N. A. Florescu, in *Transactions of the 8th National Vacuum Symposium,* edited by L. E. Preuss (Pergamon, Oxford, 1962), Vol. 1, p. 504.
[12] MKS Instruments, Inc., Andover, MA 01810.
[13] G. F. Weston, Vacuum **29**, 277 (1979).

[14] R. Holanda, J. Vac. Sci. Technol. **10**, 1133 (1973).
[15] S. Bliman, J. Aubert, R. Geller, B. Jacquot, and D. Van Houtte, Phys. Rev. A **23**, 1703 (1981).
[16] *Handbook of Chemistry and Physics, 55th Edition,* edited by R. C. Weast (Chemical Rubber, Cleveland, 1974), pp. E68,E74.
[17] C. L. Cocke, R. DuBois, T. J. Gray, E. Justiniano, and C. Can. Phys. Rev. Lett. **26**, 1671 (1981).
[18] J. H. Posthumus and R. Morgenstern, Phys. Rev. Lett. **68**, 1315 (1992).
[19] V. V. Afrosimov, G. A. Leiko, and M. N. Panov, Zh. Tekh. Fiz. **50**, 519 (1980) [Sov. Phys. Tech. Phys. **25**, 313 (1980)].
[20] J. Vancura and V. O. Kostroun (unpublished).
[21] J. Vancura and V. O. Kostroun, in *VIth International Conference on the Physics of Highly Charged Ions,* edited by P. Richard, M. Stockli, C. Lewis Cocke, and C. D. Lin, AIP Conf. Proc. No. 188 (AIP, New York, 1993), p. 113.
[22] R. E. Olson, J. Chem. Phys. **56**, 2979 (1972).
[23] R. E. Olson and A. Salop, Phys. Rev. A **14**, 579 (1978).
[24] S. S. Gershtein, Zh. Eksp. Teor. Fiz. **43**, 706 (1962) [Sov. Phys. JETP **16**, 501 (1963)].
[25] H. Ryufuku, K. Sasaki, and T. Watanabe, Phys. Rev. A **3**, 745 (1980).
[26] A. Barany, G. Astner, H. Cederquist, H. Danared, S. Huldt, P. Hvelplund, A. Johnson, H. Knudsen, L. Liljeby, and K. G. Rehnsfelt, Nucl. Instrum. Methods B **9**, 397 (1985).
[27] A. Niehaus, J. Phys. B **19**, 2925 (1986).
[28] A. Niehaus, J. Phys. (Paris) Colloq. **9**, C137 (1987).
[29] C. Froese-Fischer, Comput. Phys. Commun. **43**, 355 (1987).